Descending Reflectivity Cores in a Simulated Supercell

Leigh Orf
Department of Geology, Central Michigan University, Mount Pleasant, Michigan, USA

Matthew Gilmore
Department of Atmospheric Sciences, University of Illinois, Urbana, Illinois, USA

Jerry Straka
School of Meteorology, University of Oklahoma, Norman, Oklahoma, USA

Robert Wilhelmson
Department of Atmospheric Sciences, University of Illinois, Urbana, Illinois, USA

Louis Wicker
National Severe Storms Laboratory, Norman, Oklahoma, USA

Erik Rasmussen
Cooperative Institution for Mesoscale Meteorological Studies, University of Oklahoma, Norman, Oklahoma, USA

A three-dimensional supercell simulation using ice microphysics is presented. The storm is simulated using a non-hydrostatic numerical model initialized using a vertical sounding profile of the atmosphere above Lockney, TX, on 2 June 1995, in close time and space proximity to several tornadic supercells. The simulated supercell exhibits features similar to those observed in nearby storms on that day, including descending reflectivity cores (DRCs) as well as a tornado. DRCs and tornadogenesis are found to occur simultaneously and in close proximity. Causality is not addressed herein. Two DRCs, both of which comprise rain and are associated with downdrafts, are examined. One DRC is associated with a counterrotating shear signature during tornadogenesis, while the other occurs adjacent to a strengthening tornado.

1. Introduction

Descending reflectivity cores (DRCs) are local radar reflectivity appendages which descend from the echo overhang of the rear side of the weak echo region in supercell thunderstorms. These features were first documented in detail by *Rasmussen et al.* [2006; hereafter referred to as R06] in Verification of the Origins of Rotation in Tornadoes Experiment [VORTEX; *Rasmussen et al.*, 1994] Doppler radar data in supercells which occurred on 2 June 1995. Observations associated with this storm have also been studied in detail by *Wurman and Gill* [2000] and *Rasmussen and Straka* [2007]. DRCs were found to be associated with a velocity signature suggesting counterrotating vortices with an approximate vertical axis of rotation, and in one case, a DRC was found to coincide spatially with a developing tornado. *Kennedy et al.* [2007] performed an analysis of Level II radar data from 64 supercells occurring in the month of May from 2001–2005, and found that DRCs were common in both tornadic and nontornadic supercells, but did not find a causal relationship between DRC occurrence and tornadogenesis. As far as we know, these two papers comprise the full body of observational literature concerning DRCs to date. Much remains unknown concerning their origin and possible influence on supercell morphology.

Numerical simulations of storms in this same environment were presented by *Gilmore and Wicker* [1997], *Gilmore and Wicker* [1998] and *Auligne* [1999] who found counterrotating vortex pairs within the supercell hook region for horizontal grid spacings less than 700 meters and using three-category ice microphysics. Tornado-like circulations were also coarsely resolved; however, the origins of the DRC and vortex pairs were not investigated in those earlier studies. The thermodynamic and kinematic influence of DRCs on the sub-storm supercell environment has yet to be fully explored, and the nature of DRCs has yet to be examined numerically. This research aims to numerically simulate a supercell containing DRCs in order to do a preliminary investigation on the origins and influence of DRCs on supercell morphology, particularly with regard to tornadogenesis. Here preliminary results from a simulated supercell thunderstorm, which contains similar structure to the observed Dimmitt, Texas storm (R06) are reported.

2. Experimental Design

The Bryan Cloud Model [CM1; *Bryan and Fritsch*, 2002] is run with 100 meter horizontal grid spacing and a vertical grid stretching from 25 m to 375 m spacing over 100 levels. The model domain spans 120 by 120 by 20 km and the storm is kept near the center of the model domain using a constant storm-following box speed. The ice microphysics documented by *Gilmore et al.* [2004], which predicts two liquid and three ice habits (cloud water, cloud ice, rain, snow, and graupel/hail) is employed, and this is largely based upon the *Lin et al.* [1983] equation set. The model is initialized with a horizontally homogeneous base state taken from the Lockney, TX VORTEX sounding (See Fig. 3 from *Gilmore and Wicker* [2002]), launched shortly before the development of tornadic supercells producing DRCs. The cloud is initiated using the standard technique of a warm bubble perturbation and is run for two hours of model time. The complete three-dimensional state of the model history data is saved in five-second intervals.

Model reflectivity values are calculated from hydrometeor mixing ratios using the methodology of *Smith et al.* [1975]. The DRCs shown herein all meet the criteria set in R06, which specify the required location and structure of these features. DRCs are first identified in the supercell by animating isosurfaces of reflectivity in the regions centered about the main updraft. Reflectivity contours are then evaluated on a horizontal plane to verify that a DRC echo maximum locally exceeds 4 dB from surrounding values (following R06).

3. Results

The storm develops rapidly, exhibiting supercellular characteristics 40 minutes into the simulation, roughly corresponding to the onset of the first DRCs [*Orf et al.*, 2006]. Tornadogenesis occurs at approximately 1:40, and a single tornado forms, dissipating 12 minutes later. The tornado achieves a maximum pressure deficit of 15 mb and produces storm-relative maximum winds of $30\,\mathrm{m\,s^{-1}}$ (ground relative winds of $35\,\mathrm{m\,s^{-1}}$), which would be characterized as an EF0 on the Enhanced Fujita scale. Over two hours of storm simulation, the supercell produces several distinct DRCs. The characteristics of two DRCs and their association with the local downdrafts are now discussed.

Both of the DRCs presented here are found to comprise entirely of rain (and no ice) below 4 km. Although some DRCs might also consist of melted ice, simulations using a multi-moment microphysics scheme that tracks the rain's history confirms that similar DRCs in this part of the supercell were found to be formed primarily through collision/coalescence mechanisms [*Gilmore et al.*, 2006].

3.1. DRC D1

The morphology of DRC 1 (hereafter D1) is shown in Fig. 1. At 1:40:40 D1, indicated by an isosurface[1] of 49 dBZ, is pendant from the echo overhang, extending from 4.3 km to 1.4 km AGL. It is found along the rear flank of the supercell updraft, denoted by the gray isosurface of $\mathrm{w} = 25\,\mathrm{m\,s^{-1}}$. 50 seconds later, at 1:41:30, the bottom of D1 has descended to 0.8 km AGL and is located 700 m south of a developing vortex labeled T (indicated by the white isosurface of -3 mb pressure perturbation). 90 seconds later D1 has impinged upon the ground, coincident with the intensification of T , which maintains approximately the same horizontal distance from the center of D1. The morphology of D1 (Fig. 1) shows a strong resemblance to the observed DRC which preceded tornado formation in the Dimmitt, TX supercell (see Fig. 1 in R06).

In most cases observed by R06, DRCs near ground were found to be associated with a single-Doppler velocity feature indicating counterrotating shear (see their Fig. 4). In order to explore whether D1 is associated with similar flow, horizontal cross sections are plotted at 1.1 km AGL, the same height as the shear feature noted in Fig. 4 of R06 (see Fig. 2). D1 is enclosed by the thick green 49 dBZ contour located in the center of Figs. 2a-e at 1:43:00, the same time as denoted in Fig. 1b. Storm-relative horizontal winds in Fig. 2a indicate a similar flow pattern to that suggested by Fig. 4 in R06. D1 is embedded within a northwesterly jet, flanked on either side by winds with a significant southerly/southerwesterly component. In addition, a vertical vorticity couplet, as revealed in Fig. 2a via the gray contours, flanks D1. These features are all consistent with the counterrotating shear signature denoted by the curved cyan arrows in Fig. 4 of R06.

D1 is associated with a downdraft indicated by the $-5\,\mathrm{m\,s^{-1}}$ dashed blue contour in Figs. 2a-c. In order to explore the contributions towards vertical air accelerations in this region, a pressure forcing decomposition is performed [*Rotunno and Klemp*, 1982, 1985]. Following *Rotunno and Klemp* [1985], we decompose contributions towards nondimensional pressure π into terms involving velocity derivatives (dynamic pressure, π_{dn}) and buoyant (π_b) components, and examine each contribution towards the vertical acceleration $\frac{\partial w}{\partial t}$:

$$\left(\frac{\partial w}{\partial t}\right)_{dn} = -c_p\overline{\theta}_v\frac{\partial \pi_{dn}}{\partial z}, \quad (1)$$

$$\left(\frac{\partial w}{\partial t}\right)_{b} = -c_p\overline{\theta}_v\frac{\partial \pi_{b}}{\partial z} + B, \quad (2)$$

where c_p is the specific heat of dry air, $\overline{\theta}_v$ is the virtual potential temperature of the reference sounding, and B is buoyancy computed relative to the reference sounding. Fig. 2c indicates negative buoyancy acceleration occurs throughout D1 at 1.1 km AGL, and the orientaition of this forcing is similar to the shape of D1 and the downdraft. Dynamic pressure forcing throughout D1 (Fig. 2b) is either positive or only slightly negative. A further exploration of the contributions towards buoyancy (not shown) indicates that negative virtual potential temperature perturbation in this region contributes 70-80% of the negative buoyancy in this region, while precipitation loading contributes the remainder. At this time tornadogenesis is occurring north of D1 as indicated by the location of the -3 mb pressure perturbation contour. Further research is required to investigate whether D1 is influencing the process of tornadogenesis at this time.

The flow signature at D1 is dominated by low-level outflow at 12.5 m AGL, the lowest model vertical level (see Figs. 2d and e). At this level D1 is embedded within a northwesterly flow regime and lacks the counterrotating shear signature found at 1.1 km. D1 remains situated about 1 km to the southwest of the developing tornado vortex. Buoyancy acceleration is negative throughout the region as would be expected within the cold pool, which contains deficits of virtual potential temperature due to evaporation and melting throughout its extent. Fig. 2d reveals an association between D1 and a local drop in buoyancy immediately downwind of D1. This drop in buoyancy is spatially coincident with a region of maximum horizontal divergence indicated in Fig. 2e. The association of D1 with negative buoyancy and horizontal divergence at the surface is consistent with a negatively buoyant downdraft impinging upon the ground. The relationship between DRCs and surface dynamic and thermodynamic perturbations will be explored in future work.

3.2. DRC D2

Following the initial stage of tornadogenesis, the tornado vortex indicated by T rapidly intensifies. During this intensification, DRC D2, indicated by the 55 dBZ isosurface in Fig. 3, descends from a height of 1.2 km AGL. The white -7 mb pressure perturbation isosurface indicates the location of intensifying tornado (the same vortex shown previous figures). A three-dimensional rendering of this vortex indicates the axis of rotation of the tornado at this level is not vertically erect but is oriented with a significant northward tilt. Fig. 4 contains a horizontal cross section through the region surrounding D2. The oblong shape of the -7 mb contour, which surrounds the cyclostrophic pressure deficit within the tornado, illustrates the fact that the axis of rotation within the tornado is oriented in a northward direction (Fig 4a). The $-15\,\mathrm{m\,s^{-1}}$ contour indicates the location of the downdraft enclosed within D2. The downdraft contained within D2 is found to be consistent with the cyclonic flow about the axis of rotation of the tornado itself. Pressure decomposition analysis reveals that unlike with D1, negative vertical accelerations in this region appear to be primarily generated from dynamic pressure forcing (Fig. 4b), i.e., the pressure associated with the thunderstorm's three-dimensional velocity field, not from buoyant accelerations (Fig. 4c). In fact, buoyancy forcing is weakly positive throughout much of the downdraft bounded by the $-15\,\mathrm{m\,s^{-1}}$ contour.

4. Discussion

A supercell thunderstorm containing DRCs closely associated with tornadogenesis has been simulated and examined numerically. The morphology of the DRC examined by R06 in the Dimmit, TX, supercell is similar in morphology to the first DRC examined herein. In addition, the counterrotating shear signature found in R06 is also found 1.1 km AGL in the simulated storm, just as tornadogenesis is occurring. The first DRC is found to be associated with negative buoyancy due to temperature deficits and mass loading, and is found to contribute towards the formation of a downdraft. At the surface, this DRC is found adjacent to a region of horizontal divergence consistent with that of a negatively buoyant downdraft impinging upon the ground.

A second DRC is found to overlap with the circulation of an intensifying tornado. This DRC appears to be forced downward primarily by the circulation through via dynamic pressure acceleration rather than by way of buoyancy.

These preliminary results leave many questions unanswered and will guide our future research. Some specific questions which remain unanswered include:

1. Does negatively buoyant air associated with evaporation and precipitation loading within DRCs eventually enter the tornado? If so, what is the impact on the tornado?

2. What are the microphysical origins of DRCs? Are they formed via warm rain processes (collision/coalescence between cloud and rain drops) or due to melting of snow or hail? How do their origins affect their negative buoyancy?

3. Are DRCs responsible for creating a counterrotating shear signature? If so, how?

4. Can there be a causal link between DRCs and tornadogenesis at least in some cases?

The first two questions concern microphysics and will be approached by looking closely at microphysical source and sink terms and by analyzing trajectories within the DRC. The second two questions pertain to the dynamical influence that DRCs may have on their environment. These will be approached with techniques including Lagrangian parcel analysis techniques as well as a more rigorous exploration of the dynamical pressure equation.

Acknowledgments.
We would like to thank George Bryan, who supplied pressure decomposition code as well as model support, and Jon Siwek for programming assistance. This work was supported National Science Foundation grants ATM-9318914, ATM-0339519, ATM-0449753 and ATM-0003869, as well as the College of Science and Technology at Central Michigan University. This work was partially supported by the National Center for Supercomputing Applications under ATM040009, MCA94P023N, and TG-MCA94T023 and utilized Copper (IBM P-690), Cobalt (SGI Altix-3700), and Tungsten (Dell Xeon IA-32 Cluster).

Notes

1. DRCs, as defined in R06, may be indicated by arbitrary values of reflectivity, so long as all other DRC criteria are satisfied. The values of reflectivity selected in this paper were chosen by trial and error using interactive visualization software. It should be emphasized that a DRC isosurface does not usually represent an isolated region of precipitation bounded by precipitation-free air, but is usually, as in both examples herein, embedded within a broader region of precipitation.

References

Atlas, D., C. W. Ulbrich, and C. R. Williams (2004), Physical origin of a wet microburst: Observations and theory, *J. Atmos. Sci.*, *61*, 1186–1196.

Auligne, T. (1999), Convective storm simulation of the 2 June 1995 Dimmit, TX tornadic supercell: Comparison with observations and analysis, Master's thesis, Ecole Nationale De La Meteorologie, Note de travail de l'ENM numero 657a, 118 pp.

Bryan, G. H., and J. M. Fritsch (2002), A benchmark simulation for moist nonhydrostatic numerical models, *Mon. Wea. Rev.*, *130*, 2917–2928.

Fujita, T. T. (1985), The downburst. SMRP Research Paper 210, 122 pp. [NTIS PB-148880.].

Gilmore, M., and L. J. Wicker (1997), Dimmitt-like tornado in a simulated supercell storm of 2 June 1995. VORTEX workshop, Pacific Grove, California, 2-3 December, 1997 [Talk].

Gilmore, M., and L. J. Wicker (1998), Supercells simulated in the 2 June 1995 Western Texas Panhandle environments, in *Preprints, 19th Conf. on Severe Local Storms*, pp. 242–245, Amer. Meteor. Soc., Minneapolis, MN.

Gilmore, M. S., and L. J. Wicker (2002), Influences of the local environment on supercell cloud-to-ground lightning, radar characteristics, and severe weather on 2 June 1995, *Mon. Wea. Rev.*, *130*, 2349–2372.

Gilmore, M. S., J. M. Straka, and E. N. Rasmussen (2004), Precipitation and evolution sensitivity in simulated deep convective storms: Comparisons between liquid-only and simple ice and liquid phase microphysics, *Mon. Wea. Rev.*, *132*, 1897–1916.

Gilmore, M. S., L. G. Orf, R. B. Wilhelmson, J. M. Straka, and E. N. Rasmussen (2006), The role of hook echo microbursts in simulated tornadic supercells. Part II: Sensitivity to microphysics parameterization, in *23rd Conference on Severe Local Storms*, St. Louis, section 13.3.

Kennedy, A., J. M. Straka, and E. N. Rasmussen (2007), A statistical study of the association of DRCs with supercells and tornadoes, *Wea. Forecasting*, *22*, 1191–1199.

Lin, Y.-L., R. D. Farley, and H. D. Orville (1983), Bulk parameterization of the snow field in a cloud model, *J. Appl. Meteor.*, *22*, 1065–1092.

Orf, L. G., M. S. Gilmore, R. B. Wilhelmson, J. M. Straka, and E. N. Rasmussen (2006), The role of hook echo microbursts in simulated tornadic supercells. Part I: Association with counterrotating vortices and tornadogenesis, in *23rd Conference on Severe Local Storms*, St. Louis, section 13.2.

Rasmussen, E. N., and J. M. Straka (2007), Evolution of low-level angular momentum in the 2 June 1995 Dimmitt, Texas, tornado cyclone, *J. Atmos. Sci.*, *64*, 1365–1378.

Rasmussen, E. N., J. M. Straka, C. A. Doswell III, F. H. Carr, M. D. Eilts, and D. R. MacGorman (1994), Verification of the origins of rotation in tornadoes experiment: VORTEX, *Bull. Amer. Meteor. Soc.*, *75*, 995–1006.

Rasmussen, E. N., J. M. Straka, M. S. Gilmore, and R. P. Davies-Jones (2006), A preliminary survey of rear-flank descending reflectivity cores in supercell storms, *Wea. Forecasting*, *21*, 923–938.

Rotunno, R., and J. B. Klemp (1982), The influence of the shear-induced pressure gradient on thunderstorm motion, *Mon. Wea. Rev.*, *110*, 136–151.

Rotunno, R., and J. B. Klemp (1985), On the rotation and propagation of simulated supercell thunderstorms, *J. Atmos. Sci.*, *42*, 271–292.

Smith, P. L., C. G. Myers, and H. D. Orville (1975), Radar reflectivity factor calculations in numerical cloud models using bulk parameterization precipitation, *J. Appl. Meteor.*, *14*, 1156–1165.

Wakimoto, R. M., and V. N. Bringi (1988), Dual-polarization observations of microbursts associated with intense convection: The 20 July storm during the MIST project, *Mon. Wea. Rev.*, *116*, 1521–1539.

Wurman, J., and S. Gill (2000), Finescale radar observations of the Dimmit, Texas (2 June 1995), tornado, *Mon. Wea. Rev.*, *128*, 2135–2164.

Leigh Orf, Department of Geology, Central Michigan University, Down Science Complex 281, Mount Pleasant, MI 48858, USA. (leigh.orf@cmich.edu)

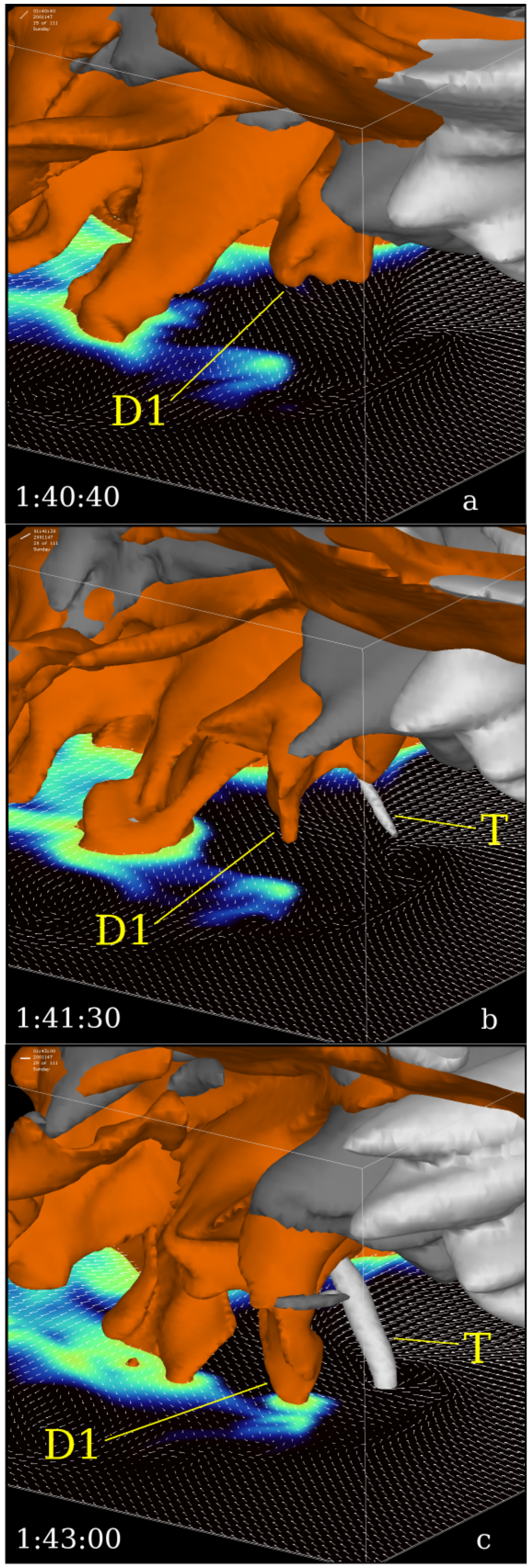

Figure 1: The evolution of DRC D1 and tornado vortex T at (a) 1:40:40, (b) 1:41:30, and (c) 1:43:00 as indicated by isosurfaces of reflectivity (orange isosurface, 49 dBZ), main updraft (gray isosurface, $25\,\mathrm{m\,s^{-1}}$), and pressure perturbation (white isosurface, -3 mb). Storm-relative surface wind vectors and reflectivity are plotted 12.5 m AGL, the lowest model level.

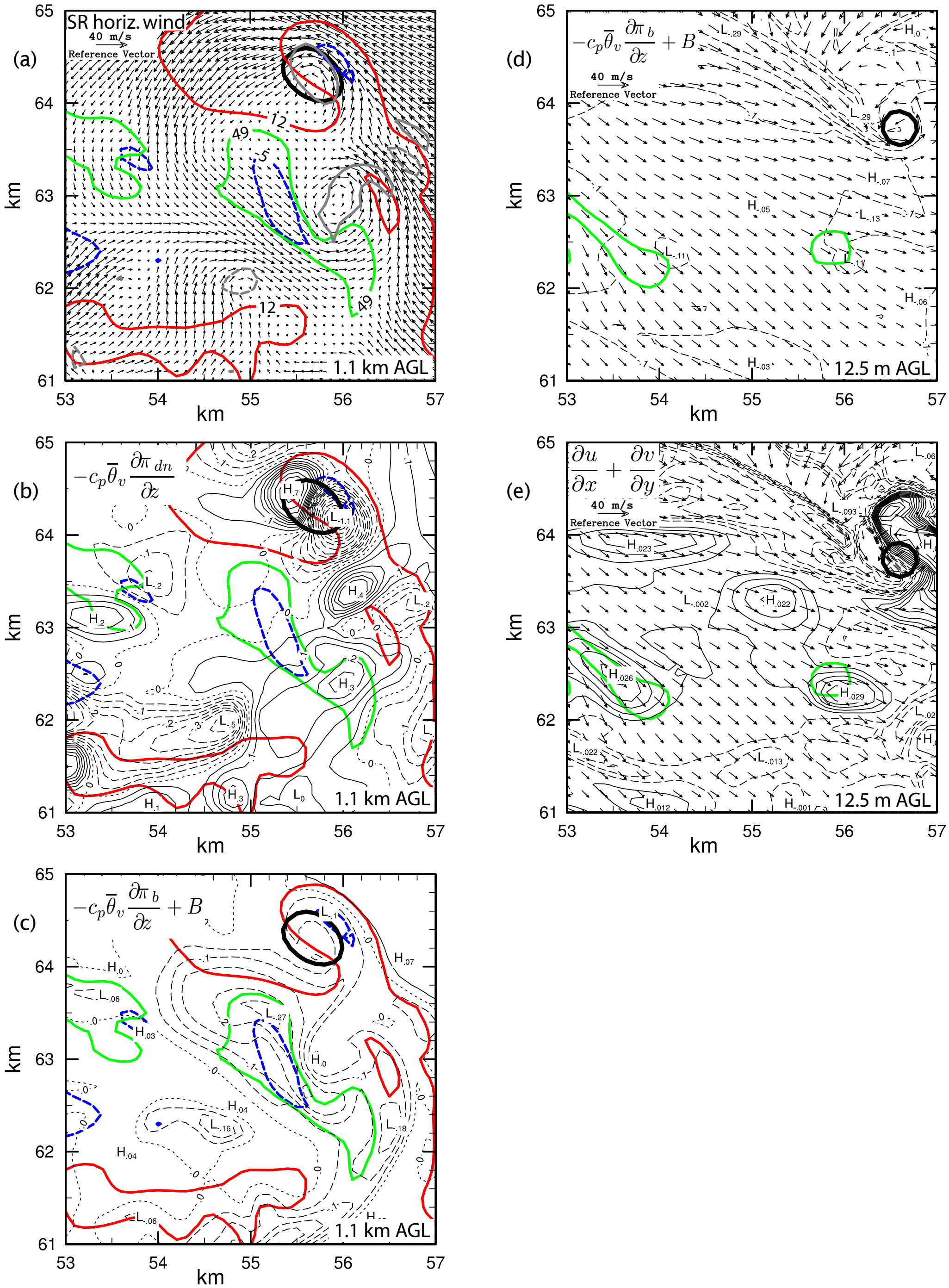

Figure 2: A horizontal cross section through D1 (49 dBZ green contour), the developing tornado (thick black contour of -3 mb pressure perturbation), downdrafts (dashed blue contour of $-5\,\mathrm{m\,s^{-1}}$), and updrafts ($12\,\mathrm{m\,s^{-1}}$ solid red contour) at 1:43:00. (a) Vertical vorticity contours of $-0.07\,\mathrm{s^{-1}}$ (dashed gray contour) and $0.07\,\mathrm{s^{-1}}$ (solid gray contour), and storm-relative horizontal wind vectors 1.1 km AGL plotted at each model grid point. (b) Dynamic pressure acceleration 1.1 km AGL. (c) Total buoyancy acceleration 1.1 km AGL. (d) Total buoyancy acceleration at 12.5 m AGL and horizontal wind vectors plotted every other gridpoint. (e) Horizontal divergence at 12.5 m AGL.

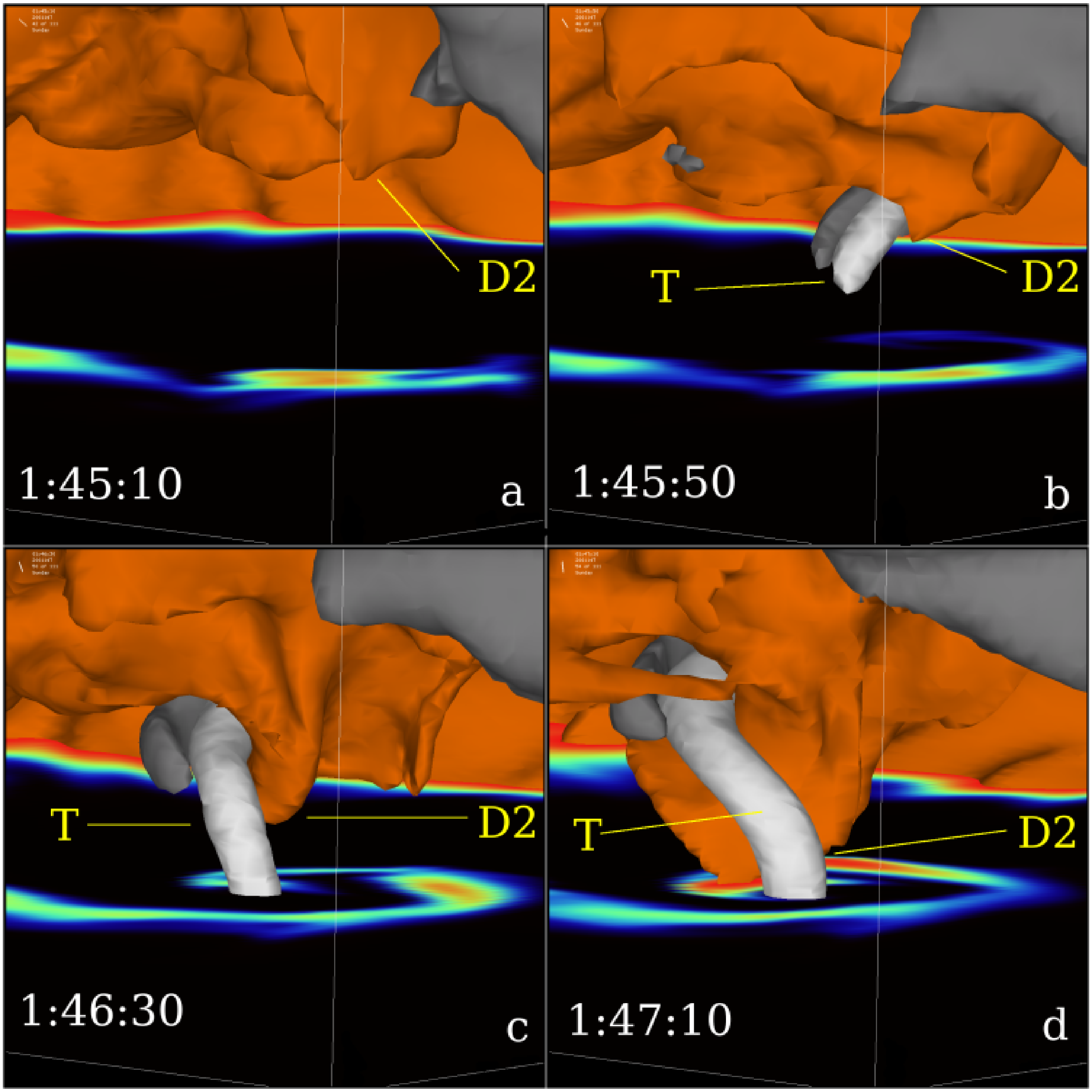

Figure 3: DRC D2 (orange isosurface of 55 dBZ), the tornado (white isosurface of -7 mb) and the main updraft (gray isosurface of $25\,\mathrm{m\,s^{-1}}$) at (a) 1:42:10, (b) 1:45:50, (c) 1:46:30, and (d) 1:47:10. Values of reflectivity at 12.5 m AGL are indicated by a colored horizontal slice.

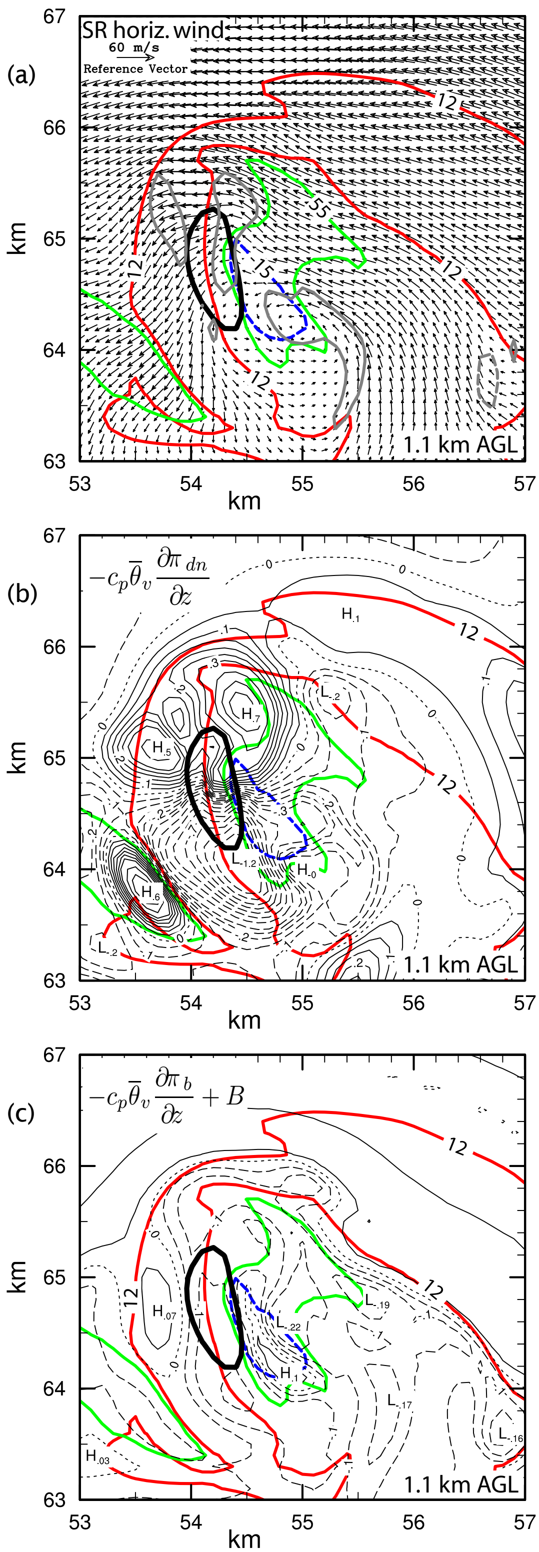

Figure 4: A horizontal cross section through D2 (55 dBZ green contour), the tornado (thick black contour of -7 mb), the main updraft (horseshoe-shaped solid red contour of $12\,\mathrm{m\,s^{-1}}$), downdraft (dashed blue contour of $-15\,\mathrm{m\,s^{-1}}$) at 1:46:30, 1.1 km AGL (2 km north of Figure 2). (a) Vertical vorticity contours of $-0.07\,\mathrm{s^{-1}}$ (dashed gray contour) and $0.07\,\mathrm{s^{-1}}$ (solid gray contour), and storm-relative horizontal wind vectors 1.1 km AGL plotted at each model grid point. (b) Dynamic pressure acceleration. (c) Total buoyancy acceleration.